Condensation in the Presence of Noncondensable Gas: the Effect of Surface Orientation

by
Ilpo Huhtiniemi

under supervision of
Prof. M.L. Corradini

Document Prepared in Partial Fulfillment for
the Requirements of the Ph.D. Preliminary Examination
in Nuclear Engineering and Engineering Physics
23 March 1990
University of Wisconsin-Madison

WESTINGHOUSE CLASS 3

Condensation in the Presence of Noncondensable Gas: the Effect of Surface Orientation

by

Tipo Hubbard

under supervision of
Prof. M.L. Corradini

Document Prepared in Partial Fulfillment for
the Requirements of the PhD. Preliminary Examination
in Nuclear Engineering and Engineering Physics
23 March 1993
University of Wisconsin-Madison

Table of Contents

List of Figures

List of Tables

1. Introduction

In the event of a reactor accident involving a pipe break, a large amount of steam may be released into the containment building. Unless measures to reduce the pressure are taken, it may exceed the structural strength of the containment and lead to a release of radioactive material. However, condensation of steam on cold containment surfaces will act as a heat sink and mitigate this pressurization. If one is to estimate the condensation heat transfer rates in such a scenario, the presence of a large amount of noncondensable gas and its suppression effect on heat transfer rates must be taken into account. This effect is due to the formation of a layer of noncondensable gas adjacent to the wall through which the steam must diffuse to condense. Therefore, the heat transfer rates are controlled by a diffusion phenomenon rather than heat conduction into the wall. If hydrogen is mixed with steam, the accumulation of hydrogen caused by condensation could also have an important implication. An accumulation of hydrogen may result and increase the risk of having a hydrogen burn.

External cooling of the containment to suppress pressurization is possible, if the containment structure allows reasonably effective heat transfer rates through the wall to an ultimate heat sink. Notably, the Westinghouse Electric Corporation has adopted this kind of a passive water cooling system for its AP-600 nuclear power plant design to

provide a heat transport path to the atmosphere. The AP-600 design incorporates large capacity water tanks placed on top of the containment building which are drained onto the containment dome in the event of an accident. The system is gravity-driven and thus fully passive. Once the tanks are drained, the natural circulation of air will continue to provide cooling. Westinghouse Electric has begun experimental research efforts to determine the efficiency of this passive containment cooling system.

In the recent years, the research in condensation at the University of Wisconsin has focused on studying condensation heat transfer under conditions that may be expected in a severe accident. This work has continued under contracts from the Department of Energy and Westinghouse Electric Corporation. Current research effort is largely based on the theoretical work performed by Kim [1] on turbulent film condensation and the experimental work on the effects of interfacial waves on condensation by Barry [2]. The apparatus constructed by Barry also was used to conduct scoping experiments on condensation on inclined surfaces that helped the design of the new test section. The results from these experiments were published by Huhtiniemi [3].

The goal of current study is to use the experimental results to address the following questions in condensation heat transfer in a containment geometry:

- what is the magnitude of condensation heat-transfer coefficients

- the effect of surface orientation and
- the effect of the prevailing conditions
  - flow field
  - mass ratio of air and steam
  - pressure
- the effect of the condensing surface

A thorough understanding of physical phenomena and the effect of scaling is required before extrapolation of the experimental results to larger scales can be attempted.

A brief review of previous investigations of the factors affecting condensation is given in the next chapter. The reported research of condensation phenomena under accident conditions is scarce. Therefore, a proposal of an experimental research project is introduced to remedy a lack of experimental results.

2. Previous Investigations

The objective of this chapter is to briefly review the published literature on the condensation phenomena and, specifically, the factors that are of importance for the current research effort. For more exhaustive literature reviews the reader should consult the reviews by Kim [1] and Barry [2]. The published experimental work can be divided into two categories from the containment safety perspective:

1) **separate effects tests**, where an effect of one or a few selected parameters were studied,
2) **integrated (large scale) tests**, where the obtained results have engineering value, but do not mechanistically address all the phenomenon involved.

In the following two chapters some of the pertinent observations are reported, so that results of the current research effort can be compared with existing observations. The large scale experiments provide valuable background information about physical conditions for the small scale experiments and their results can be used to benchmark the physical models. Therefore, the design and the results of some of the large scale experiments are discussed.

2.1 Separate Effects Experiments

The practical applications of condensation processes, in which a large amount of noncondensable gas is present, are few. The bulk of the literature, in which the effects of noncondensable gases have been studied, *the mass ratio* of noncondensable gas to the vapor has been low (W_{inf} = 0.0001 - 0.01). Generally, the heat transfer coefficients are observed to decrease dramatically with increased noncondensable gas mass fraction [2,3,4,5].

The experimental work with noncondensable gases has been typically conducted with stagnant gas/vapor mixture, because it is more amenable to analysis. Cho and Stein [3] and Kroger and Rohsenow [5] have reported that a one-dimensional diffusion theory gives results that agree well with the experimental ones. However, their analysis is not valid when a significant amount of natural convection exists. Turner and Mills [7] studied the condensation of mercury vapor in the presence of air. *A forced convection flow* resulted in higher heat transfer coefficients, because of the sweeping effect of the flow. Forced flow also induces interfacial instabilities that increase the heat transfer rates [2].

The dropwise condensation mode leads to heat transfer coefficients that are one order of magnitude larger than in filmwise mode in case of pure vapor [10]. However, the dropwise condensation in the presence of noncondensable gas has gained very little

attention, because of the difficulties in getting reproducible results [3,10,11]. The dropwise condensation on a inclined surface was studied by Chiba et. al.[6]. They found that the drops rolling down the surface increase the heat transfer coefficient. The increase is attributed to a sweeping effect that exposes a bare surface, where new drops can grow. However, when the surface coverage of falling drops increases, the heat transfer rate starts to decrease. Therefore, Chiba concludes that the heat transfer coefficient is a function of the surface renewal frequency and the distance downstream from the leading edge of the condensing plate.

The surface finish has a major effect on the mode of the condensation [14]. There has been considerable interest in finding a surface finish that can sustain a dropwise condensation mode for long periods of time. The wetting characteristics of the surface ultimately determine the mode of condensation. The dropwise condensation is likely to exist on non-wetting surfaces and filmwise is likely on wetting surfaces. In dropwise condensation mode with polished metal surfaces the heat transfer characteristics are likely to change due to oxidation of the surface or tarnishing [11].

The geometry and, in particular, *the orientation of the surface* affects the dynamics of the condensation phenomena. The two important factors that have an effect on the dynamics are:

1) **the stability of condensate interface** which is dependent on the interfacial shear and the orientation of the surface
2) **natural convection** which is dependent on the bouyancy forces and orientation of surface

Barry [2] studied the effects of interfacial structure caused by shear. He reported that enhanced mixing, which is caused by the interfacial structure, mitigated the effect of the noncondensable gas.

Only a few studies have been performed with an arrangement in which the condensing surface is facing downwards with varying inclination angle. Gerstmann and Griffith [4] studied the condensation of the pure, stagnant Freon-113 and water vapor at atmospheric pressure. The test plate was ma. e of 2 inches thick copper plate (18 by 6 inches). Both heat transfer measurements and visual observations were made. They observed several distinct flow regimes in the condensate film depending on the angle of inclination. In the horizontal position the condensate interface consisted of a random array of "cosine-shaped" pendant drops. The drop density was observed to increase with the heat flux. The development of a transient dropwise condensation pattern was observed which indicated that the boundaries of the surface had a strong effect during the transient. In the steady state case the boundaries appeared to have a neglible influence. In the case of an inclined surface the authors observed three different flow regimes; 1) a smooth and waveless

interface close to the leading edge, 2) region of developing waves (elongated drops or longitunal ridges) and, 3) a fully developed region, which is independent of the downstream distance and inclination, consisting of "roll waves". These regions were observed in all non-horizontal cases. However, the behaviour in these regimes changed with inclination angles between 7.5-20°. No changes were observed with the angles greater than 20°.

Cho and Stein [3] investigated the condensation of steam on a copper plate in the presence of air and helium. The steam and gas mixture was stagnant. The condensing surface was facing downwards and its area was 15 cm^2. The system pressure was varied from 0.31-1.24 MPa. The experiment showed that the natural convection would be the dominant mass transfer mechanism in a stagnant system with air as a noncondensable gas. Cho and Stein were able to correlate data reasonable well using an analogy between heat and mass transfer. The Nusselt number for mass transfer was correlated as a function of Rayleigh number. The results with helium corresponded with analytical estimates only with small helium concentrations. The discrepancy between theory and observed results with higher helium concentrations were attributed to a fog generation and its motion. Fog generation was observed also with air as a noncondensable gas, but no effect was reported in that case. The increase of *the system pressure* was observed to increase the heat transfer rates. Pressure was also reported to have a complicated effect on the mode of condensation in the presence of helium.

2.2 Large Scale Experiments

Westinghouse Electric Corporation conducted a test series that demonstrated the feasibility of their containment cooling system concept [19]. The water film behaviour, mass transfer (evaporation), and convective heat transfer on the external surface was investigated experimentally. Furthermore, the overall condensation heat transfer rates were measured. These results can be used in verification of the CWNG models. Therefore, a brief description of the experimental apparatus is given in the following paragraph with some reported results.

The facility consists of a 24 foot tall, 3 feet in diameter pressure vessel containing air or nitrogen at one atmosphere. The schematic drawing of the apparatus is shown in Fig. 1. The amount of injected steam was varied so that the pressure in the system varied from 1.69 bar to 6.52 bar. Saturated steam was throttled to the pressure vessel through three different kinds of steam distributors. One of them is illustrated in Fig. 1, this diffuser provided a slow radial distribution of injected steam uniformly into the vessel. The other configuration was a conical diffuser at the end of steam supply pipe. It was used at two different locations so that the mixing of air/steam by the buoyant plume and the density stratification effects could be studied. The heat flux was measured locally by thermocouples (24 pairs). The overall heat flux was computed from the difference between injected steam and drained condensate enthalpies. The thermocouple arrangement

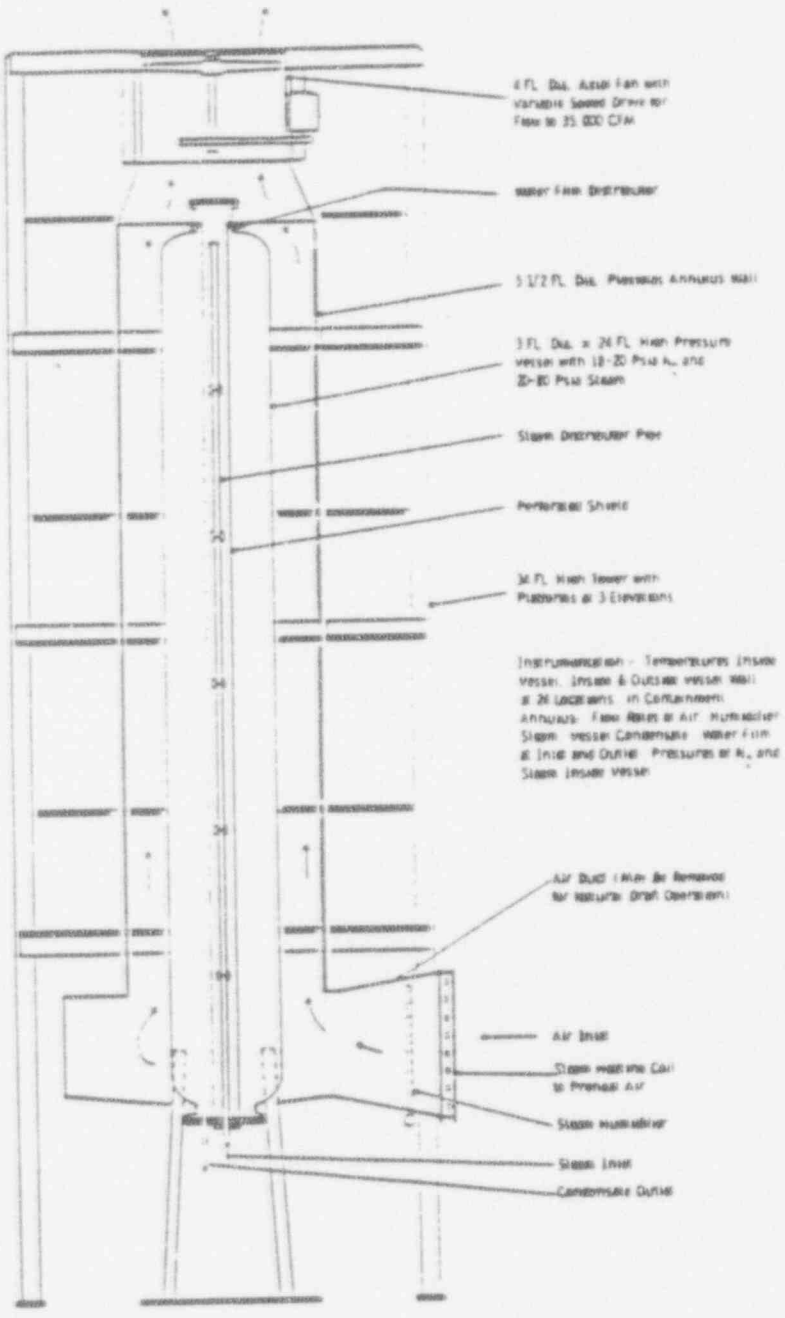

Figure 1 Experimental Apparatus used by Westinghouse Electric Corp. [19]

consisted of two thermocouples, one inside of the vessel's three-eights of an inch thick steel wall and one on the outside.

The results for the wetted surface runs are shown in Fig. 2. These results are the averages over the total condensing area. A clear dependence of results on the location of steam diffuser can be seen. The location has a strong effect on the mass ratio of the resulting steam/air mixture and the velocity of the flow pattern inside the vessel. It was reported that the local measurements consistently underpredicted the overall heat removal, the reason for this was not reported.

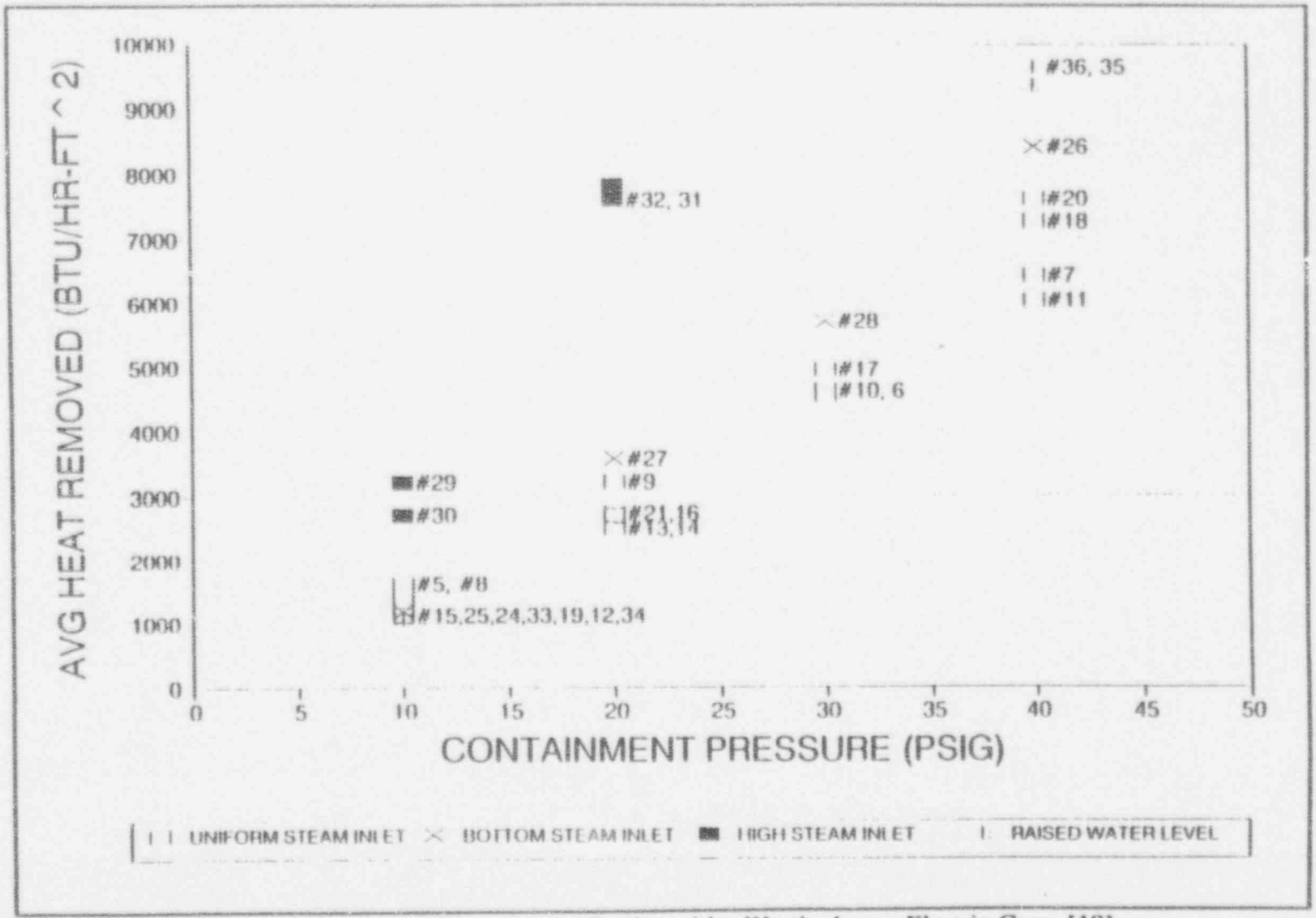

Figure 2 Results of Experiments Conducted by Westinghouse Electric Corp. [19]

3. Research Proposal

3.1 Goal of the Proposed Reseach Effort

The goal of this research effort is to study condensation in the presence of a non-condensable gas and determine the heat transfer coefficients under the conditions that are likely to exist in a containment in a reactor accident. The physical state of the system under study is very different compared to the bulk of other reported condensation experiments performed in the past. Each of the reviewed previous investigations address only a part of the physics in the condensation process and the results have only a qualitative value. Therefore, a set of experiments is required in order to compose a complete physical picture of condensation phenomena under the accident conditions in a containment and to get quantitative information about the heat transfer rates.

The reviewed literature suggests that the following factors are of importance for the current study:

- Geometry (scaling) and orientation of the condensing surface
- Noncondensable gas concentration (gas/vapor mass ratio)
- Bulk velocity

- Pressure
- Surface finish

Each of these factors is considered in the proposed research effort. However, the emphasis is placed on understanding the effect of the orientation and the scaling on the results. The results and observations are used to create a physical picture of condensation phenomena. The physical picture is then used as a basis of a simple modelling effort. The experimental work and analysis to achieve the stated goals are discussed in the following chapters.

3.2 Scope of the Proposed Research Effort

3.2.1 Experimental Work

The experimental work is divided into two phases: AP600-1 and AP600-2. The test matrixes for the AP600-1 and AP600-2 are given in tables 1 and 2, respectively. Both sets of experiments provide quantitative data about the effects of orientation, mass fraction and velocity. The AP600-2 is also used to study the effect of pressure in the range from 1-2 bar. Qualitative observations of the scaling and surface effects are made by comparing AP600-1 and AP600-2 series data. Furthermore, both the test series provide a visual access to the mixture flow and the test surface. Qualitative information about the flow

TABLE 1 Test Matrix for AP600-1

		VELOCITY		
TEMP	m_{air}/m_{steam}	1 m/s	2 m/s	3 m/s
60	6.6			therm-23,24,26,26,48,49,59
70	3.6		therm-19,20,21,22,50,58	therm-8[1],10[1],12,13,16,17,47,57
80	1.8	therm-27,28[1],29[1],30,31,51,55	therm-9[1],11[1],15,14,18,45,46,56,61,62	therm-32,33,34,35,52,60
95	0.3	therm-36,37,38,39,40,41,42,43,44,53,54		

The effect of inclination was measured at: 0°, 6°, 12°, 20°, 45°, 72° from horizontal.

TABLE 2 Test Matrix for AP600-2

		VELOCITY		
TEMP	m_{air}/m_{steam}	1 m/s	2 m/s	3 m/s
60	6.6			0°,6°,12°,20°,90°
70	3.6	0°,6°,12°,20°,90°		
80	1.8	0°,6°,12°,20°,90°		
90	0.7	0°,6°,12°,20°,90°	0°,6°,12°,20°,90°	
100	~0	0°,6°,12°,20°,90°	0°,6°,12°,20°,90°	
110	0.5	0°,6°,12°,20°,90°	0°,6°,12°,20°,90°	
110	2	0°,6°,12°,20°,90°	0°,6°,12°,20°,90°	
120	0.5	0°,6°,12°,20°,90°	0°,6°,12°,20°,90°	

patterns and the condensate behaviour is essential for the analysis of the results.

The experimental work in the AP600-1 phase has already been completed. This phase was conducted with the existing condensation test facility. The detailed description of the setup can be found in [8]. The results and observations of this "scoping" set of experiments are given in the following chapter. Then the work in AP600-2 phase is discussed.

3.2.1.1 AP600-1 Test Series

RESULTS AND DISCUSSION

Over sixty tests were conducted. A goal of measuring the heat transfer coefficient with an uncertainty less than 10 percent was satisfied for most data. An error analysis of data showed that the uncertainty was about 7 percent using the heat-flux-meters and about 9 percent using the energy-balance method. The error analysis assumed that the thermal properties were known precisely; i.e. uncertainty was solely determined by measurement accuracy. In the following discussion the heat-flux-meter method is favored, because of some unexpected difficulty in obtaining reliable coolant flow measurements caused by the valves regulating the coolant flow. These uncertainties were dependent on the each coolant loop and the flow rate in that particular loop. These systematic errors in heat-flux-meter data and flow data are to be addressed in the AP600-2 set of experiments.

The surface temperature was obtained by performing a least-squares-fit with the measured temperatures in the plate and then extrapolating the surface temperature. An effort of maintaining a constant surface temperature throughout the test series was made to minimize the error encountered in such an extrapolation. A surface temperature value of 30 °C was chosen to minimize the losses outside (room temperature varied 25°-30° C). However, it was found that obtaining an exactly uniform surface temperature by adjusting coolant flows and temperatures was not possible in most tests, because very high heat-transfer rates at the beginning of the plate. Generally the surface temperature varied over a maximum range of 28°-32° C across the length. The small variations in average surface temperatures were not found to affect the heat transfer results.

The results are summarized in table 3. In figures 3-6 the results for the heat transfer coefficient as a function of location along the plate are given. The reader should note that the non-labelled set of data refers to 72° inclination angle. The effect of temperature (or the mass ratio) can be seen by comparing figures 3 and 4 (or 5 & 6). The heat transfer coefficient increases with mixture temperature as expected. It is interesting to note that the curves for different inclinations are closer together in Fig. 4. In Fig. 1 there is a notable difference in between inclination angles 6° and 12°. This is an indication of a transition from having stationary droplets to an onset of rivulet formation (confirmed by visual observations). However, it was not fully understood why the similar behavior was not seen with increased flow velocity Fig. 5 for a mixture temperature of 70° C.

TABLE 3 AP600-1 Results

RUN	MIX TEMP [°C]	WALL TEMP [°C]	VEL [m/s]	ANGLE [°]	CEB RESULTS [W/m²K]	HFM RESULTS [W/m²K]

a,b

RUN	MIX TEMP [°C]	WALL TEMP [°C]	VEL [m/s]	ANGLE [°]	CEB RESULTS [W/m²K]	HFM RESULTS [W/m²K]

a, b

RUN	MIX TEMP [°C]	WALL TEMP [°C]	VEL [m/s]	ANGLE [°]	CEB RESULTS [W/m²K]	HFM RESULTS [W/m²K]

a,c

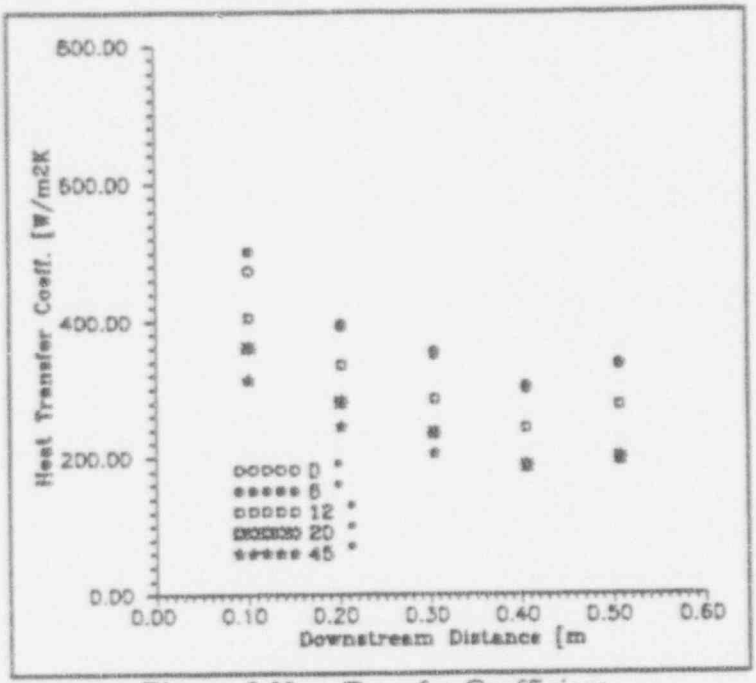

Figure 3 Heat Transfer Coefficient
(T_{min}=70°C, v=2 m/s)

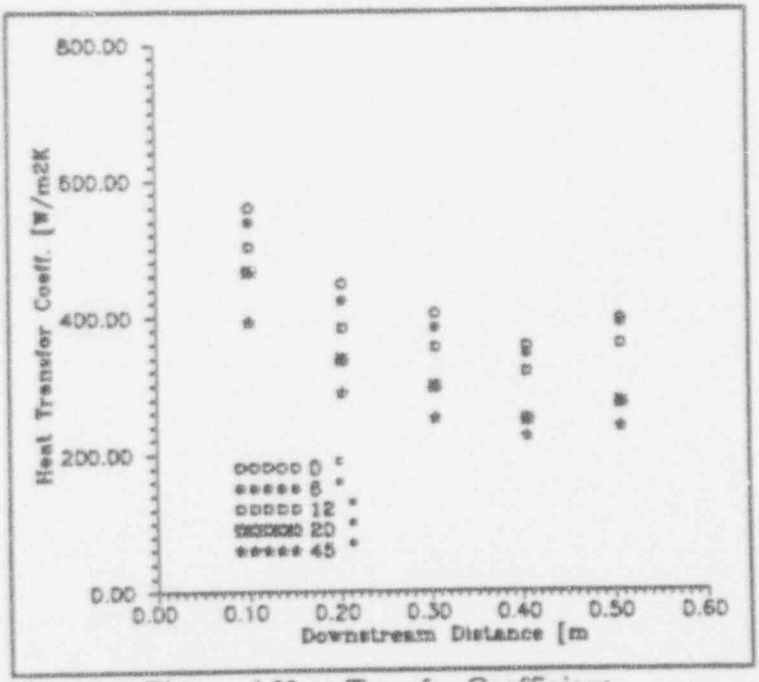

Figure 4 Heat Transfer Coefficient
(T_{min}=80°C, v=2 m/s)

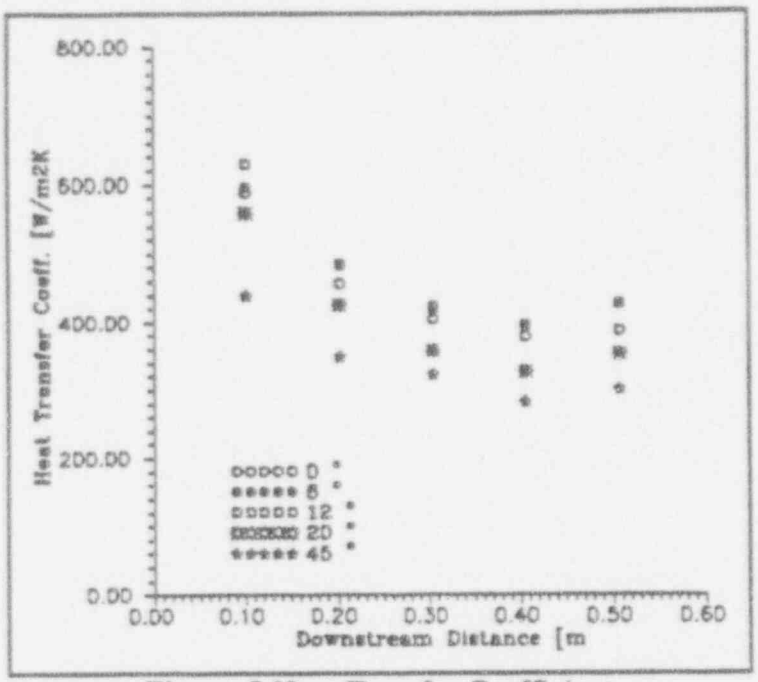

Figure 5 Heat Transfer Coefficient
(T_{min}=70°C, v=3 m/s)

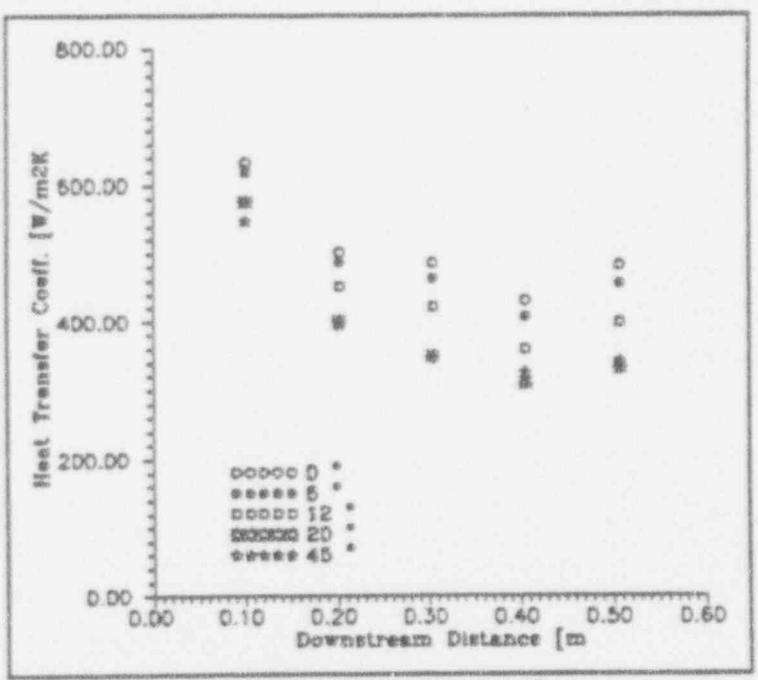

Figure 6 Heat Transfer Coefficient
(T_{min}=80°C, v=3 m/s)

The trend of decreasing heat transfer rate is caused by a developing noncondensable gas boundary layer. The heat transfer is controlled by the diffusion of steam through this layer. The small increase in heat flow rate in the trailing edge of the plate is due to heat flow to the plate from the hose flange structure. A teflon plate was used as an insulation, but it proved to be inadequate. A heat conduction analysis indicates that the heat transfer coefficient is overestimated by 5-10% due to this. However, there is still a possibility that an additional mechanism exists, that leads to an enhanced heat transfer rates. AP600-2 experiment should resolve that issue.

In Fig. 7 heat transfer coefficients (average value over the plate) are plotted as a function of the inclination angle. If the decrease in heat transfer coefficient is attributed to rivulet formation and a change in the gas flow pattern, it can be seen that the transition occurs between 6 - 12° inclination. This was also confirmed by visual inspection. The mixture velocities (1-3 m/s) were not high enough to sweep the droplets down the plate in the horizontal position. Uniformly distributed droplets existed with rivulets even with the higher inclination angles. No visually observable condensate film existed at any inclination, which indicates either a very thin film or lack of wetting on the metal surface. The results from low mass-ratio runs (92°-95° C) did not indicate dependence on the inclination angle (Fig. 8). However caution should be taken in interpreting these results, because of the difficulties in reaching the desired steady initial conditions. The repeatability of these runs was poor compared to runs with a mass ratio bigger than one,

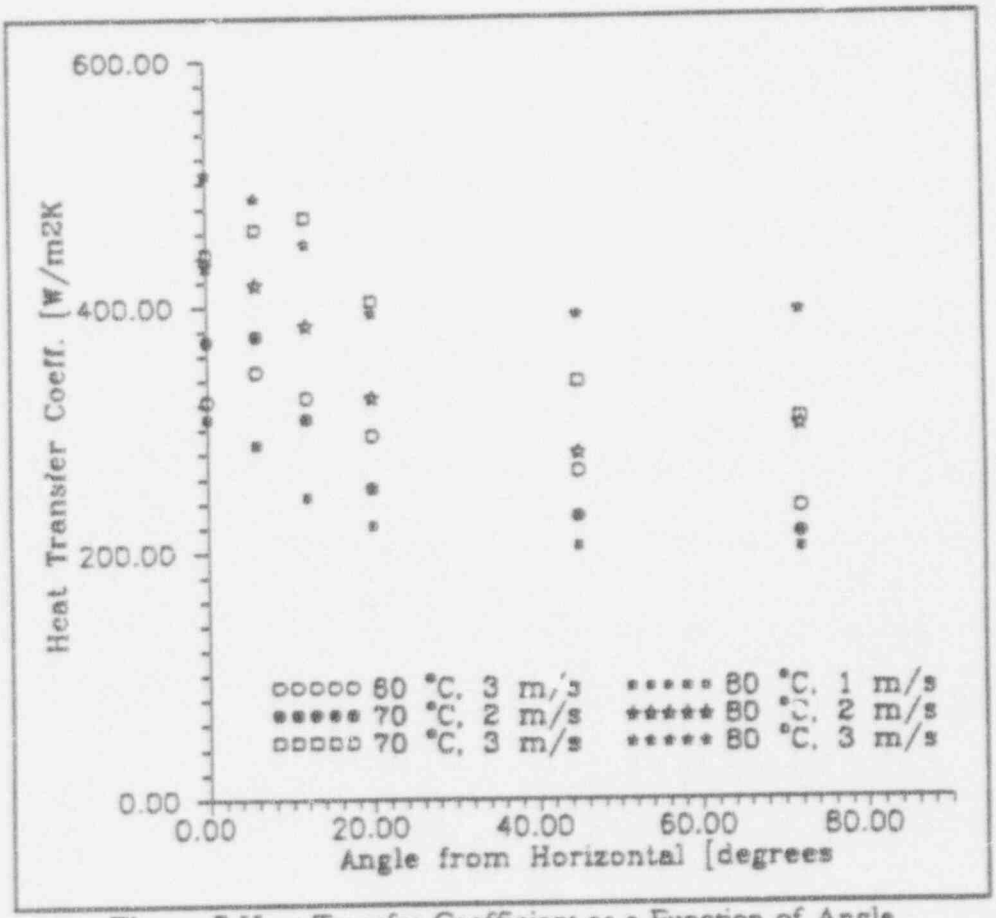

Figure 7 Heat Transfer Coefficient as a Function of Angle

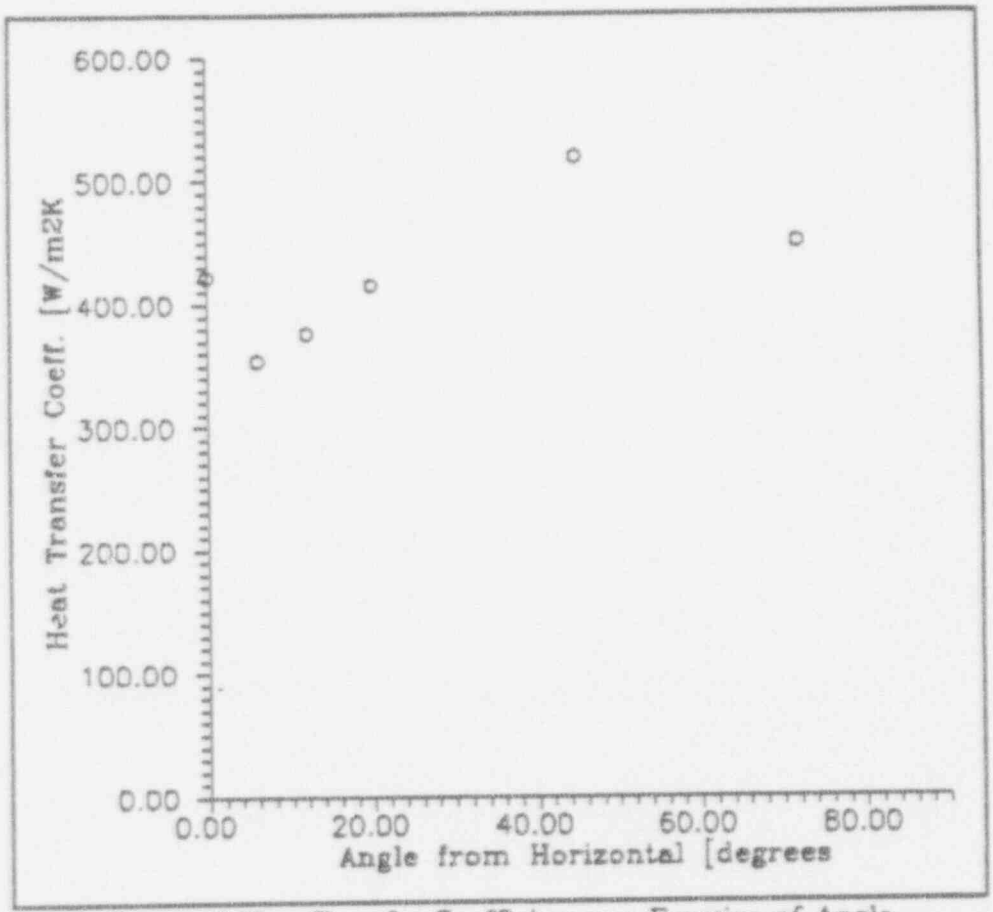

Figure 8 Heat Transfer Coefficient as a Function of Angle
(T_{mix}=94 °C,v=2 m/s)

because of the variation of the initial air/steam temperature (mass ratio) and its effect on the condensation rate. The heat flux axial profiles are flattened as expected, because little noncondensable gas was present.

The effect of mixture flow velocity can be seen in Fig. 9 for a mixture temperature of 80° C. The heat transfer coefficient increases monotonically with increasing the mixture velocity. As the results were compared with the previous study made by Barry [2] a considerable difference was found between the observed heat flows for inclination angles of 0° and 130°, Fig. 10. Extensive checks with experimental procedures were made, but the difference persisted. The following physical causes were examined:

a) a surface effect in which the spaces between large droplets are covered with thin films that result in higher heat transfer rates,

b) increased surface area, because the surface is covered with droplets (i.e. droplets acting as fins),

c) bulk gas mixing caused by raining droplets,

d) a natural circulation flow pattern perpendicular to the mixture axial flow direction.

A simple approach had to be adopted to study a surface effect. A test with similar conditions was repeated with a surface covered some deposit that had accumulated during

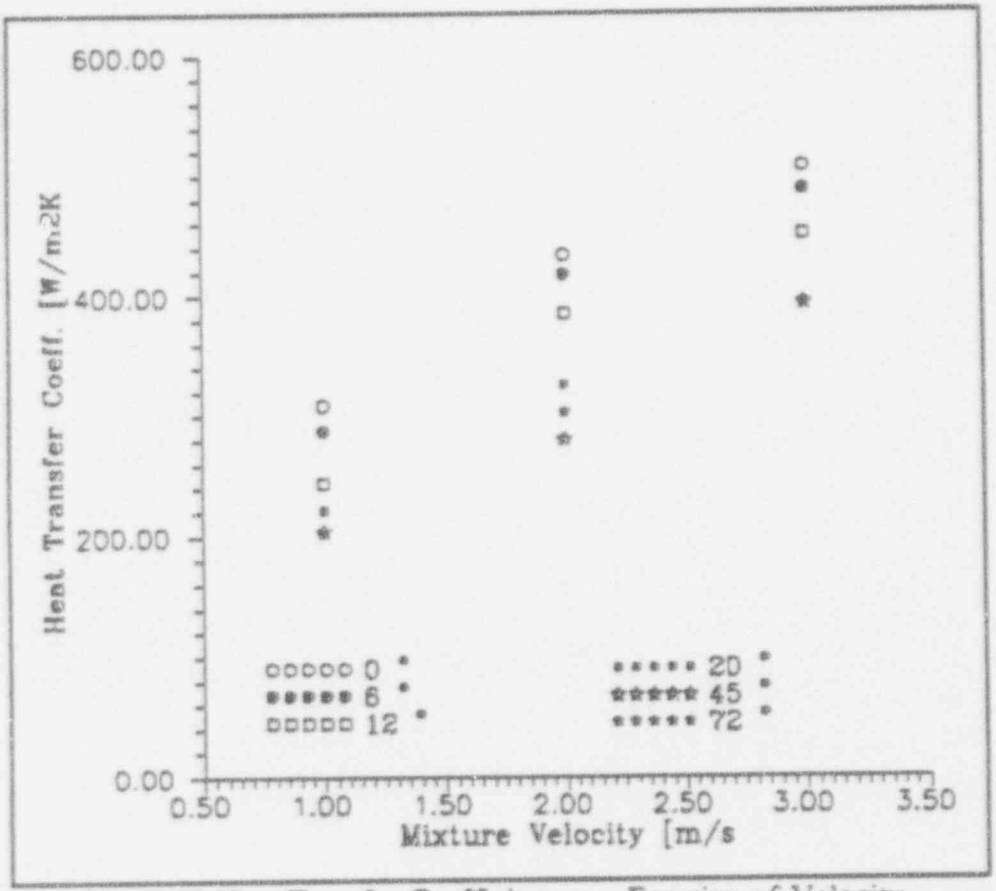

Figure 9 Heat Transfer Coefficient as a Function of Velocity (T_{min}=80 °C)

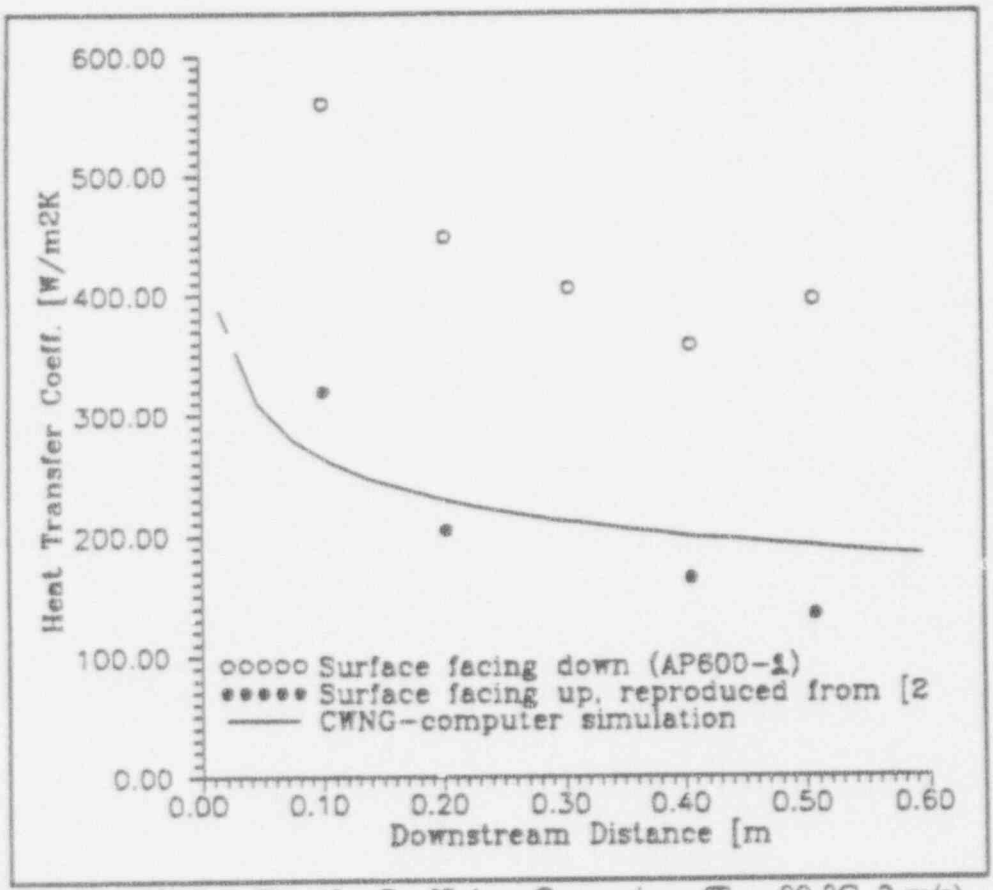

Figure 10 Heat Transfer Coefficient Comparison (T_{mix}=80 °C, 2 m/s)

the series of experiments and with a thoroughly cleaned surface. All these results are well within error margins indicating that at least the contaminants on the plate surface have no effect. The AP600-2 set of experiments are conducted with a plate having a prescribed surface finish. The comparison between the results and observations can give us qualitative information about surface finish.

As the plate was tilted the number of droplets decreased. Unless the droplet size distribution was considerably shifted towards very small droplet sizes, the increase of heat transfer rates due to fin-effect seems to be unlikely, because even with a smaller number of droplets the heat transfer rates were higher than observed by Barry. As the inclination was increased and droplets were rolling down the surface rather than raining down heat transfer rates decreased, but were still higher than Barry's.

By eliminating the former hypotheses as a source of discrepancy, the natural circulation pattern developing in the channel might be a likely explanation. However, in this series of runs the facility was not equipped with necessary instrumentation to make observations of a two-dimensional flow pattern occurring at a particular location of the test section. A simple hand calculation using a dimensionless parameter, Gr/Re^2, to estimate the natural convection importance was performed. The computed values (0.0001 - 0.001) indicated that forced convection dominates. However, the AP600-2 set experiments with additional instrumentation and flow visualization test runs is going to address the issue of secondary

flow pattern. If a natural circulation pattern is proved to be the source of enhanced heat-transfer rates, care must be taken to model and scale the experimental results, because of the strong coupling of described phenomena to the scale. It is not expected that the Maragoni effect is important here since the gas fraction is large.

CONCLUSIONS

A condensation heat transfer tests were performed in the presence of non-condensable gas with varying surface inclinations. The following observations can be drawn from the results of the first test series. First, as our past experiments [2] indicate the condensation heat transfer coefficient increases as the mixture velocity increases or the the air/steam mass ratio decreases. Second, as one increases the angle of inclination the heat transfer coefficient decreases. During these tests we made visual observations to determine the flow pattern of the condensate on the cold wall and found stationary droplets dripping from the wall until angles of 6 - 12°. Beyond this point the condensate formed droplets which coallesced into rivulets that drained down the metal cold wall. The maximum size of these droplets was less that 20 mm which is good agreement with one expects from Rayleigh-Taylor instabilities. The behaviour of the condensate had the same characteristics as reported by Gerstmann and Griffith in pure steam environment. The unexpected observations of significantly higher heat transfer rates than reported by Barry and the increasing heat transfer rates at the end of the plate gave additional impetus in continuing the research effort with improved facility. The proposed work with the new facility are

discussed in the next chapter.

3.2.1.2 AP600-2 Test Series

The AP600-2 test series is planned to give quantitative results of the heat transfer rates under the same conditions as AP600-1 as well as at pressures ranging from 1-2 bars (test matrix given in table 2.) The low temperature runs (60-80°C) are essentially repeats of the AP600-1 runs. The runs are repeated in order to get a consistent set of experiments with a new facility. Furthermore, the AP600-2 facility with improved instrumentation should be able to resolve the question of augmented heat transfer rates that were observed with AP600-1. The comparison of the results with the same test conditions is also going to provide information about the effect of scaling and the surface finish.

The effect of the system pressure is studied with two different noncondensable mass-ratios. The low air mass-ratio run is done without any injection of noncondensable gas. In that case the noncondensable gas in the system is essentially the dissolved air in the boiler feedwater. Qualitative information of the importance of the natural circulation can be obtained by comparing the low and high mass-ratio runs.

Each of the indicated runs in AP600-2 test matrix are repeated with five different inclination angles ranging from 0°-90° from a horizontal downward facing position.

Visual observations are performed in order to obtain a qualitative description of the condensate behaviour. The following observations are of interest:

- mode of condensation
- pendant drop size and behaviour
- behaviour of condensate film as a function of inclination angle

In addition to these observations, a flow visualization run will be made to determine if a significant secondary flow exists.

3.2.2 Analysis of Results

The analysis of the AP600 results consists of the following steps

- identification of the dominant factors affecting the heat transfer rates
- identification of the factors affecting scaling of the experimental results to a actual containment geometry
- implementation or refinement of the models in CWNG-computer code
- verification of the CWNG implementation using the data from AP600 test and from a large scale experiment

The CWNG-code is to be used as the basis for the modelling effort. The CWNG-code was developed by Kim [1] in his thesis at the University of Wisconsin. It is an one-

dimensional film condensation model that utilizes the analogy of the momentum, heat and mass transfer. The CWNG calculates heat fluxes through the liquid film and gas boundary layer with an assumed interfacial temperature. The interfacial temperature is then iterated until the heat fluxes converge within a specified accuracy. The heat transfer coefficient for the gas mixture consists of two contributions; convective heat transfer and the condensation

$$h_{gas} = h_{conv} + h_{cond} \tag{1}$$

The heat transfer coefficients are estimated using the following correlations

$$Nu_x = 0.0296 Re_x^{0.8} Pr^{1/3} \tag{2}$$

$$Sh_x = 0.0296 Re_x^{0.8} Pr^{1/3} \tag{3}$$

The turbulent Prandtl/Schmidt numbers are derived from the transport equations for the turbulent kinetic energy

$$Pr_t = 0.85 + \frac{0.012}{Pr} \tag{4}$$

$$Sc_t = 0.85 + \frac{0.012}{Sc} \tag{5}$$

Correction factors have been implemented in the CWNG for an apparent suction effect caused by high mass transfer rates.

The heat transfer coefficient for the liquid film is determined from Nusselt's analysis

$$h_{film} = 0.943\left(\frac{\rho_l(\rho_l-\rho_g)g i_{fg} k_l^3}{\mu L(T_l-T_{wall})}\right)^{1/4} \tag{6}$$

The CWNG also incorporates a model for the effect of interfacial waves.

The current models in the CWNG agree well with the data reported by Barry as illustrated in Fig. 10. However, a comparison with the data from AP600-1 test series implies that models in the CWNG have to be revised for the downward facing geometries. As noted in the discussion of AP600-1 results, the mechanism behind the augmented heat transfer rates is not yet known. It is expected that AP600-2 will provide the experimental data to resolve this, so that an effort of improving the CWNG models can be made.

In order to apply the results from the experiments and analysis (CWNG-code) to a larger scales and, in particular, to an actual containment geometry, several factors have to be

considered. Some of the more obvious factors are

- the difference between simple flat plate flow simulated in the experiment and the radially symmetric flow field expected in a containment
- the difference between the length scale of the experiment and real containment
- the effect of continuous curvature
- three-dimensional effects: secondary flows in the containment

In this study the goal is to address, to some extent, the first three factors. The last factor would require a scale model of the containment structure or a detailed three-dimensional flow simulation, which are beyond the scope of this research effort.

4. Experimental Facility

4.1 Experimental setup

The experimental facility that is being used in the test series consists of a test section and necessary auxilliary equipment; a boiler, air blower and secondary condenser. The process diagram is given in Fig. 11.

The design is based on experiences accumulated in using the preceding condensation research facility. The design goals were as follows;

1) approximate two-dimensional planar geometry,
2) allow heat flux measurements in the wall,
3) allow pivoting of the test section from horizontal to vertical position,
4) provide a flexible design to change the aspect ratio of the flow channel,
5) allow the pressurization of the test section (up to 1 bar gage pressure),
6) allow visual observations of the flow and condensate behaviour,
7) provide convenient access to the flow for a variety of instrumentation.

In this chapter a brief overview of the design considerations and equipment capabilities are given.

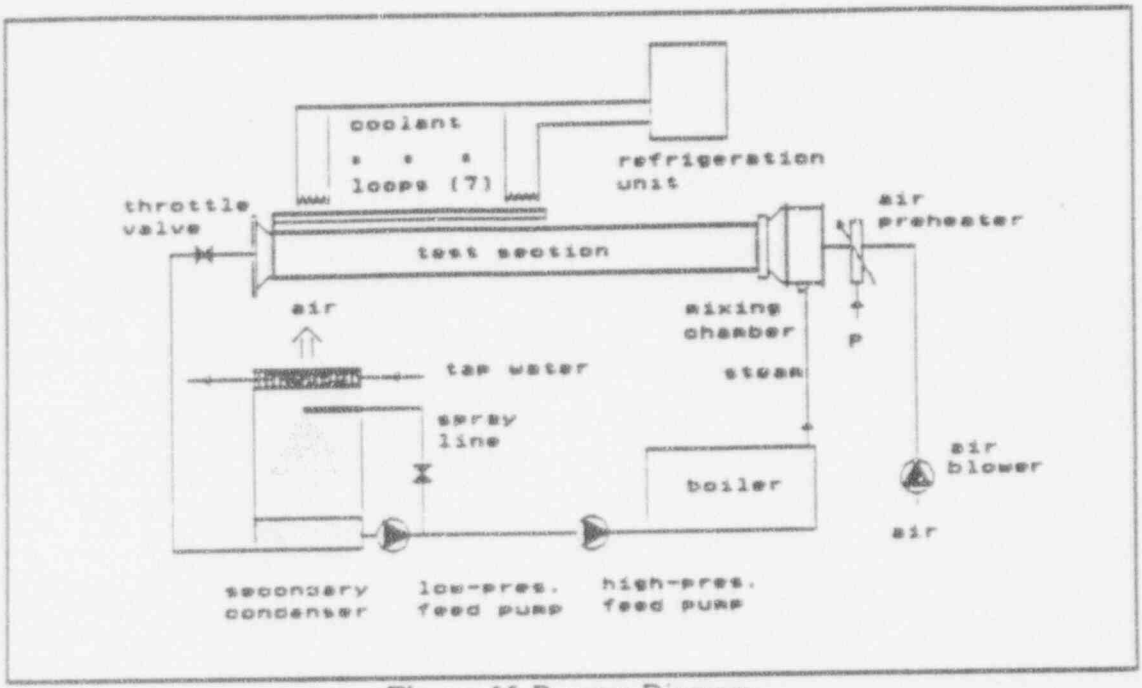

Figure 11 Process Diagram

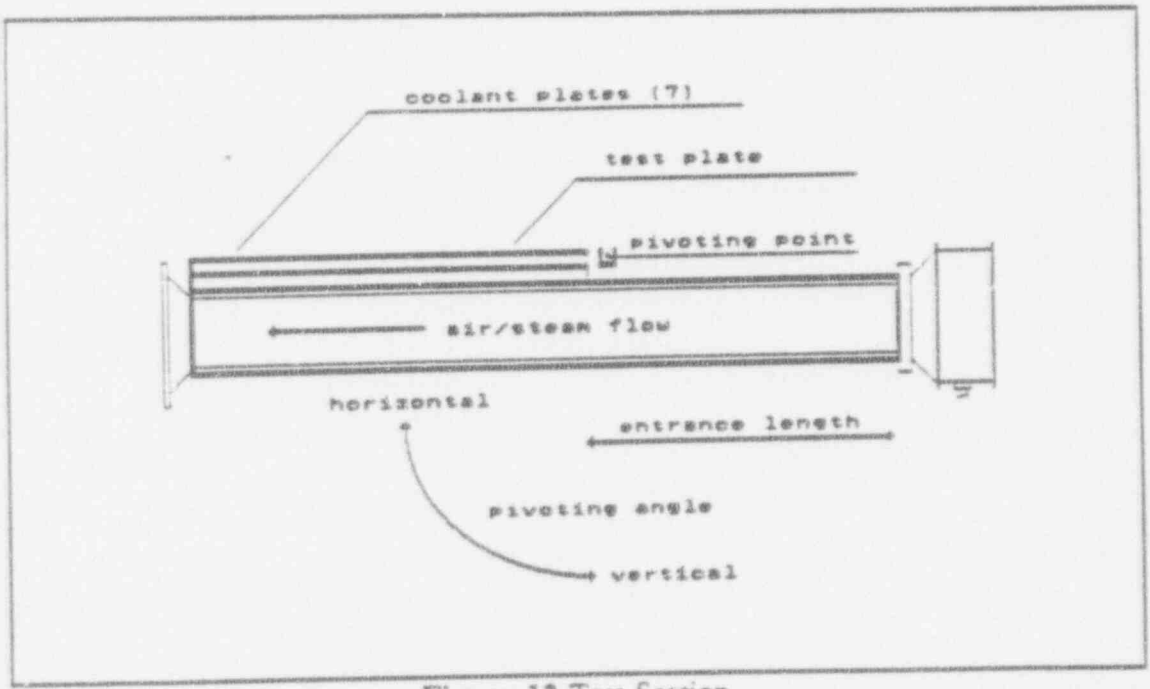

Figure 12 Test Section

The test section consists of a 109.50 cm long sandwiched clear Lexan (polycarbonite)-plates. These plates form a square duct of 15.24*15.24 cm aside. The test section was designed to withstand test temperatures of 140 °C and test gage-pressure up to 1 bar. The pivoting-point and direction of the test section is given in Fig. 12.

The first 83.82 cm of the test section serves as an entrance length. This length is considered to be long enough so that the turbulence profiles are well developed (the free stream turbulence intensities were considerably smaller than in the boundary layer close to wall). The total length of the test section is scaled so that the boundary layers of the opposite walls do not interact. Both of these design considerations are important in order to satisfy the goal of simulating a planar geometry.

The measurements take place in the section following the entrance length. This section consists of the 3.81 cm thick aluminum plate mounted as the ceiling of the duct. The arrangement is illustrated in Fig. 12. This section is simulating a portion of the containment wall. The aluminum plate is 106.68 cm long and the effective width of the heat transfer area (the area exposed to air/steam flow) is 15.24 cm. This results in an effective heat transfer area of 0.1626 m^2. The length of the plate was increased 75% over the old design because of desire to confirm the asymptotic behaviour of the heat flux. The surface finish on the plate was applied by Westinghouse Electric. The surface was sandblasted and painted with [ ]^{a,b} which will be used by Westinghouse

Electric in their AP-600 design, for the interior of the containment steel shell.

The cooling of the test wall is provided by seven independent coolant plates mounted on the backside of the aluminum plate shown in Fig. 12. These coolant plates contain a spiral flow channel machined on one side. The geometry is illustrated in Fig. 13. Water recirculated through Neslab HX-150 is used as coolant.

The Neslab HX-150 refrigeration unit is rated to supply a cooling power of 4500 W at 20 °C. This cooling enables one to maintain a 27.68 kW/m^2 average heat flux through the test wall. This is considered to be enough for the initial test phase where the air/steam ratios are ~1 or bigger. Another Neslab HX-150 unit is reserved to provide additional capability to handle test wall heat fluxes up to 50 kW/m^2.

The steam flow is provided by Reimers RH-36 boiler. The power of the boiler is 36 kW and it is rated to produce 0.0156 kg/s steam at 100 °C. The capacity of the boiler is believed to enough for the initial phase of the test series. The purchase of a new boiler is being planned for the second phase of the test series. The new boiler will, at a minimum, double the present steam capacity.

The air flow is provided by a conventional furnace blower. A blower rating is not available, but air velocities of 6 m/s were attained. These velocities are of the order of

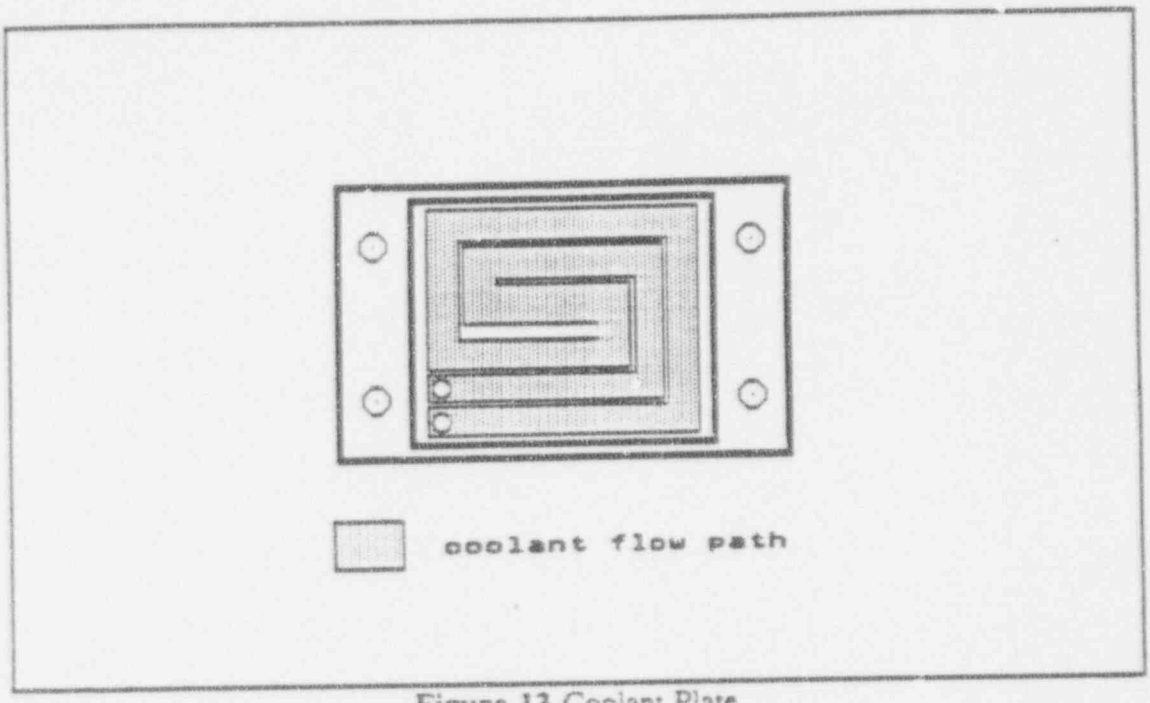

Figure 13 Coolant Plate

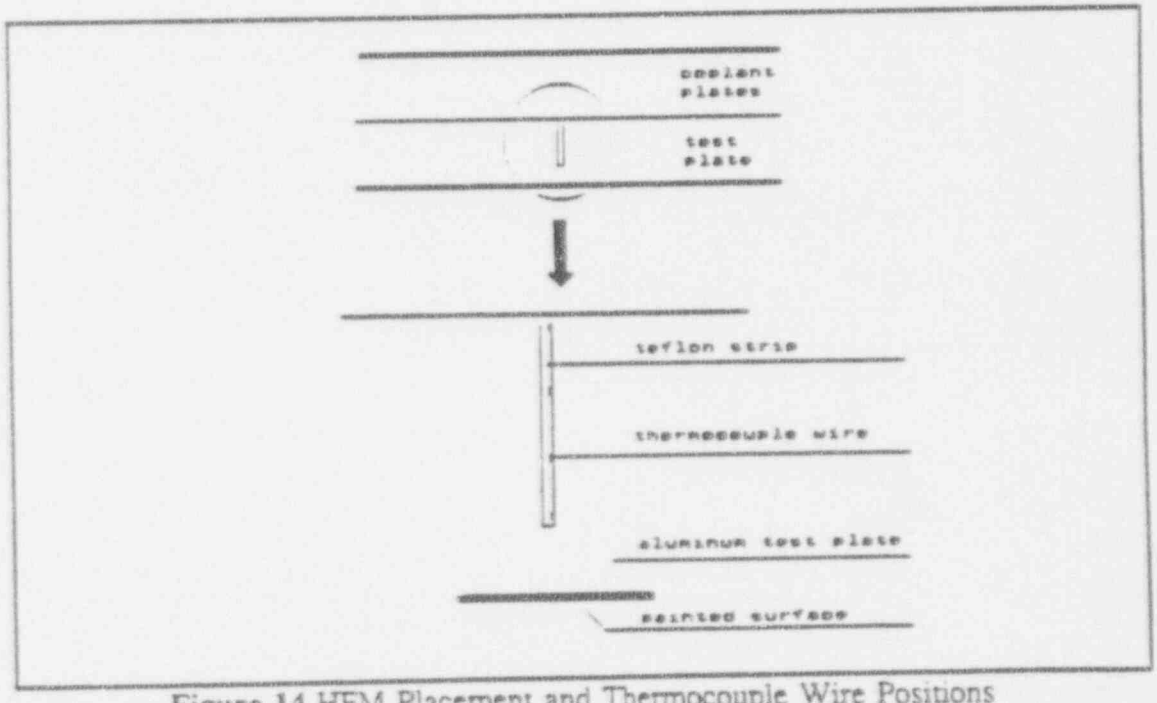

Figure 14 HFM Placement and Thermocouple Wire Positions

magnitude required.

A second unit of similar design is reserved for the pressurized runs in the event that more power is required.

The secondary condenser is used to condense the steam that flows through the test section. The unit is open to the atmosphere, thus allowing air to escape. Therefore, if pressurized conditions in the test section are desired, a throttling valve is required between the secondary condenser and test section. The steam is condensed using a spray system and a dehumidifier unit which is cooled by tap water. The feedwater from the sump is pumped back to the boiler. The inventory of circulating water lost through the dehumidifier is compensated by a flow of demineralized water from a make-up water tank.

2.2 Measurements and Instrumentation

The experimental facility has a variety of instruments in order to set the test conditions and to acquire data and make observations. The overall goal in performing the measurements was that the error of observed heat fluxes and heat-transfer-coefficients would be less than ten percent. In this chapter a brief description of test procedures is given. The measurements are also discussed with a short overview of the instrumentation.

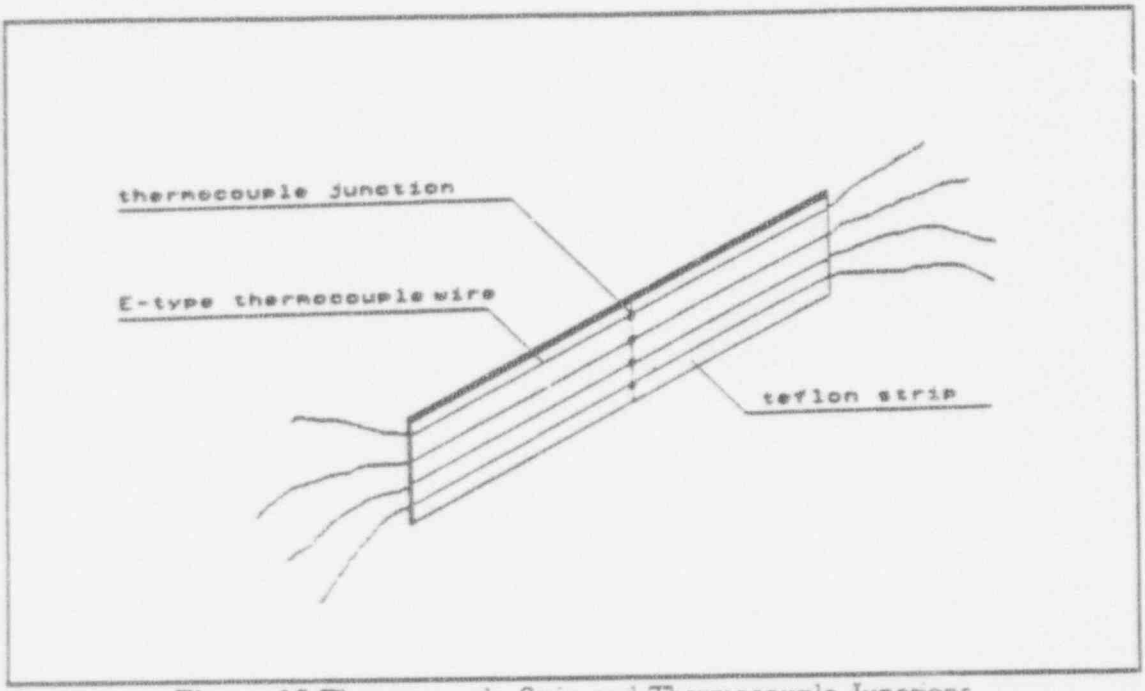

Figure 15 Thermocouple Strip and Thermocouple Junctions

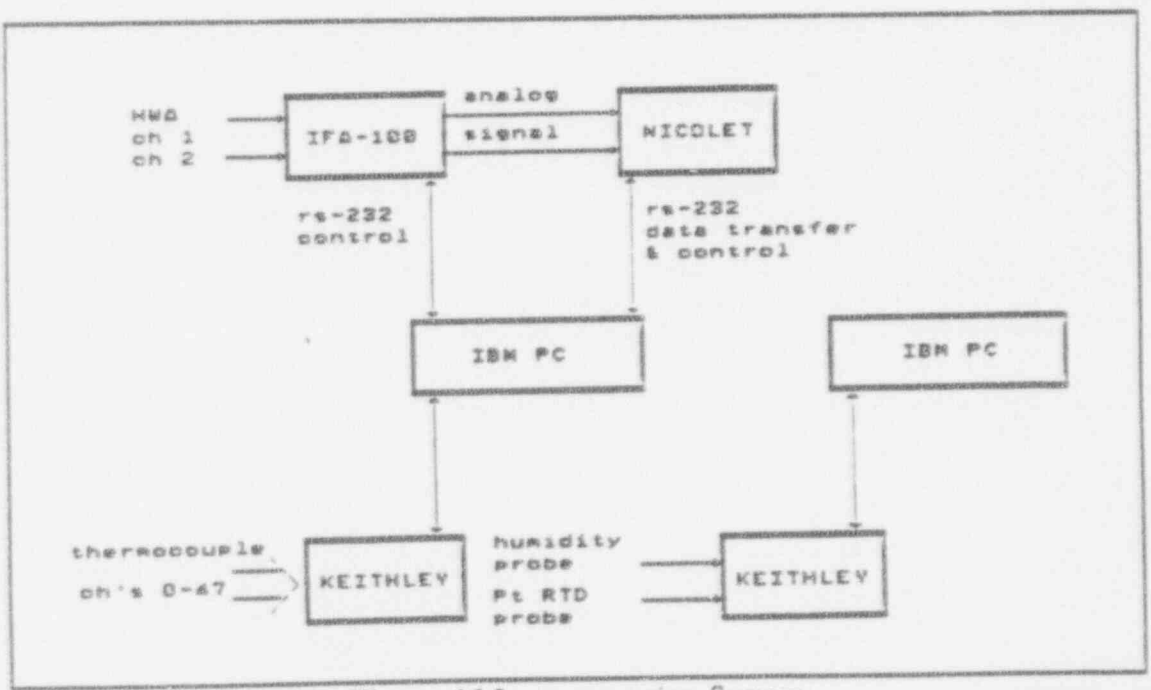

Figure 16 Instrumentation System

The experimental procedure is based on experience gained by operating the previous condensation research facility. A set of simple computer programs are used to find the right settings for the air blower speed and steam mass flow rate. The mass flow rate of steam is measured using an orifice flow meter which was assembled using regular ASME standards. Air flow is set using a pitot tube. Steam is run through the test section for at least half an hour prior to measurements so that steady state conditions are achieved. Afterwards, a set of preliminary data is taken using heat flux meters in order to check that the desired test wall surface temperature is reached. Test channel conditions are continuously monitored during data acquisition. The data is taken and averaged over 10 minute intervals.

The major interest in this test series is to find the heat fluxes through the wall as a function of orientation of the surface. The condensation heat-transfer-coefficients may be calculated from the heat flux results

$$h_{con} = \frac{q''}{T_{mix} - T_{wall}} \tag{7}$$

The heat flux measurements are accomplished using two different methods; 1) with Heat Flux Meters (HFM) or 2) calculating the Coolant Energy Balance (CEB). The principle behind both the methods is straightforward.

The HFM's consist of an array of four type-E thermocouples (wire 0.254 mm dia). The thermocouples are placed in the grooves machined on 1.59 mm thick teflon plates. The teflon strip provides support for the assembly. The locations of the thermocouple junctions on the teflon strips were recorded carefully ($\Delta x = \pm 0.05$ mm). The strips were placed into slits on the backside of the test wall. The arrangement is illustrated in Fig. 14, 15. The temperature gradient in the wall can be obtained from the thermocouple readings. Therefore, if the thermal conductivity of the aluminum is known, and if one-dimensional heat flow and steady state conditions are assumed, the heat fluxes are given by

$$q'' = k\frac{\Delta T}{\Delta x} \tag{8}$$

The thermal conductivity was measured by Properties Research Laboratory [15] an was reported to be 1.213 ± 0.006 $Wcm^{-1}{}^{\circ}C^{-1}$.

The CEB-method involves measuring the flow rates (V) through the individual coolant loops. In addition to flow rates, the ΔT_c between the inlet and outlet of each coolant loop is required. Now writing the energy balance equation, an expression for q'' can be obtained

$$q'' = \frac{Q}{A} = \frac{V \rho c_p \Delta T_{cool}}{A} \tag{9}$$

where A is the heat transfer area, c_p the specific heat, and ρ density of water.

The coolant flows in the CEB-method are measured by Dwyer Ratemaster RMC-141 flowmeters. The flowmeter is certified to have accuracy better than 2 percent of the full scale reading. All the thermocouple data is acquired by a Keithley 500-system with three thermocouple input boards which have 16 channels each. Since the experiment is running at steady state conditions, the required data acquisition rates are all well within the capabilities of Keithley 500 system. Data is stored and processed in an IBM PC computer.

In addition to heat flux data, a set of measurements is required to establish that desired test conditions prevail in the test channel. The diagnostics include a Vaisala HMP-135 thin-film humidity probe and a platinum RTD temperature sensor. This sensor combination may be used to check the gas mixture conditions at different locations in the channel. The probe is connected to the second Keithley 500 system. Two independent data acquisition systems are required so that the gas mixture humidity/temperature data can be acquired simultanously with heat flux measurements. A block diagram of the data acquisition system is given in Fig. 16.

A TSI IFA-100 hot-wire anemometer is used to measure flow fields in the test channel. The velocity field maps yield important information of flow behaviour in the channel. In particular, it is important to know if the cool wall creates a natural circulation pattern

perpendicular to flow. This circulation flow would create a definite effect that is related to geometry of the channel. The velocity maps and varying of the aspect ratio of the flow channel should address the question of circulation. The signals from the IFA-100 are digitized in a Nicolet 4094A digital oscilloscope. The bandwidth of the oscilloscope is 2 MHz and it has 16kB of memory. The Nicolet oscilloscope is well suited to acquire turbulence data because its sampling rates are high. The digitized data from Nicolet is transferred to IBM PC for further processing.

The mean velocity in the test section is also measured using a Dwyer 3.175 mm miniature pitot-tube and Dwyer model 424-5 Inclined-Vertical Manometer. However, in the near saturated steam flow conditions the pitot tube tends to get blocked by condensate droplets.

4.3 Experimental Procedure

In this chapter a brief outline of the experimental procedure is given. Prior to each experiment the HTS-computer program is run in order to estimate the air and steam mass flow rates and the air preheat power. The estimate is based on solving the energy and mass balance equations for the mixing process, which is assumed to be ideal.

The pitot tube at the exit of the test channel is used to set the correct air mass flow rate. The velocity is measured at the centerline of the test channel. The velocity profile is

assumed to be uniform across the channel. After the air mass flow is set, the steam flow is mixed with the air flow. The steam mass flow is measured with an orifice flow meter before the steam flow enters the mixing chamber. If the mixing process is close to ideal, the conditions in the test section should match the desired values: $T_{mix}=T_{sat}$ and relative humidity $\phi=100\%$. These values are checked with an RTD temperature sensor and with the humidity sensor. Scoping experiments showed that a small correction to the air blower speed is required, because of the back pressure created by the steam flow. This adjustment is done using a pitot tube. After the adjustment the mixture flow rate and the mixture temperature should correspond the estimated values. A quick check has been made to estimate the accuracy of the settings and the losses due non-ideal mixing and conduction of heat to the structure. The analysis (given in Appendix) showed that no unexpected heat losses occurred. The temperature and the coolant flow through each coolant plate is adjusted so that an uniform surface temperature profile of the test plate is achieved. This ensures that the heat flow in the plate is one-dimensional. After the coolant flow settings have been found to give the desired surface temperature, the experiment is run continuously for 1 hour in order to assure that the steady state conditions have been reached. Finally, the data is acquired over a ten minute period. Due to the limitations of the data acquisition system only 16 channels of data can be acquired simultaneously. Therefore, the data acquisition is spread over one and half hour: 10 minutes of data acquisition, 20 minutes of data transfer for each of the three 16 channel cards. The scoping experiments have shown that the long overall data acquisition period

is not a concern once steady state conditions has been reached. The mixture temperature and humidity measurements are performed simultaneously with the heat flux data acquisition. The data is then reduced using HTF-program. The measured temperatures and flow rates are then used with VEL-program to make a more accurate prediction of the mixture velocity.

References

1. M. H. Kim, *Modelling of Condensation Heat Transfer in a Reactor Containment*, PhD Thesis, University of Wisconsin, 1986

2. J. J. Barry, *Effects of Interfacial Structure on Film Condensation*, PhD Thesis, University of Wisconsin, 1987

3. D. H. Cho, R. P. Stein, *Steam Condensation on the Underside of a Horizontal Surface*, Proc. of Third Int. Topical Meeting on Nuclear Power Plant Thermal Hydr. and Operations, Nov. 1988

4. J. Gerstmann, P. Griffith, *Laminar Film Condensation on the Underside of Horizontal and Inclined Surfaces*, Int. J. Heat Mass Transfer, vol. 10, pp. 567-580, 1967

5. D. G. Kroger, W. M. Rohsenow, *Condensation Heat Transfer in the Presence of a Non-condensable Gas*, Int. J. Heat Mass Transfer, vol. 11, pp. 15-26, 1968

6. Y. Chiba, M. Suzuki, S. Ohtani, *Heat Transfer in Dropwise Condensation of Steam-Effect of Falling Drops*,

7. R. H. Turner, A. F. Mills, V. E. Denny, *The Effect of Noncondensable Gas on Laminar Film Condensation of Liquid Metals*, Trans. ASME J. Heat Transfer, vol. 95(1), pp. 6-11, 1973

8. I. K. Huhtiniemi, *Condensation in the Presence of a Noncondensable Gas: The Effect of Surface Orientation*, Proc. 26th National Heat Transfer Conference, vol. 85(269), pp. 205-210, 1989

9. C. L. Henderson, J. M. Marchello, *Film Condensation in the Presence of a Noncondensable Gas*, Trans. ASME J. Heat Transfer, vol. 91(3), pp. 447-50, 1969

10. D. W. Tanner, D. Pope, C.J. Potter, D. West, *Heat Transfer in Dropwise Condensation at Low Steam Pressures in the Absence and Presence of Non-condensable Gas*, Int. J. Heat Mass Transfer, vol. 11, pp. 181-190, 1968

11. T. G. Sundararaman, T. Venkatram, *Heat Transfer during Dropwise Condensation of Steam in the Presence of Non-coondensable Gases-Effects of Geometrical Shape of the Surface Reversal of Cooling Water Flow & Orientation*, Indian Journal of Technology, vol. 14, pp. 313-321, 1976

12. N. V. Suryanarayna, G. L. Malchow, *Film Condensation on Inclined Plane*

Surfaces,

13. L. Sledgers, R. A. Seban, *Laminar Film Condensation of Steam Containing Small Concentrations of Air*, Int. J. Heat Mass Transfer, vol. 13, pp. 1941-1947, 1970

14. A. Yamauchi, S. Kumagai, T. Takeyama, *Condensation Heat Transfer on Various Dropwise-Filmwise Coexisting Surfaces*, Trans. of JSME, vol. 51(B), pp. 2606-2613, 1985

15. R. Taylor, H. Groot, J. Larimore, *Thermal Conductivity of an Aluminum Alloy (2024)*, Properties Research Laboratory, PRL 803, 1989

16. KEITHLEY Inc., Keithley Series; Measurement and Control System, Rev. D, P/N 500-904-01, 1987

17. G. Box, W. Hunter, J. Hunter, Statistics for Experimenters, Jonn Wiley & Sons, 1978

18. TSI Inc., IFA-100 System Intelligent Flow Analyzer Manual, Rev. B, P/N 1990237, 1983

19. Westinghouse Electric Corp., *Tests of Heat Transfer and Water Film Evaporation from a Simulated Containment to Demonstrate the AP600 Passive Containment Cooling System*, NSE-90-0013, January 1990

APPENDIX

Error Analysis of Coolant Energy Balance Results

The heat flux results are obtained using the following equation

$$q'' = \frac{Q}{A} = \frac{\dot{V}\rho c_p \Delta T_{cool}}{A} \tag{1}$$

The physical properties ρ, c_p of water as well as area A are assumed to be known accurately. This means that the error in results is generated only by the measured quantities V and ΔT.

The error of the flowmeter reading V is less than two percent of the full scale reading. This is certified by the manufacturer, Dwyer Instruments Inc. The error of the temperature rise ΔT is caused by the uncertainty of the measured temperatures T_{in} and T_{out}. By using the error propagation formula we get the cumulative uncertainty

$$\Delta T_{err} = \sqrt{(T_{err_{in}}^2 + T_{err_{out}}^2)} \tag{2}$$

In this case the absolute accuracy of the thermocouple is not important, because the difference between two thermocouple outputs is measured. Therefore one can assume that the uncertainty can be traced to the resolution of the measurement. The resolution of A/D-conversion is stated to be 0.150 °C/count [16] with an E-type thermocouple. This value was used for T_{em}. The uncertainties were calculated:

$$V_{em} = 1.2618 \text{ cm}^3/\text{s}, \qquad \Delta T_{em} = 0.2121 \text{ °C}.$$

The error propagation formula with the equation (1) gives the relative error

$$\frac{q''_{em}}{q''} = \sqrt{\left(\frac{\Delta T_{em}}{\Delta T}\right)^2 + \left(\frac{V_{em}}{V}\right)^2} \tag{3}$$

A criteria can be obtained for minimum flow rates and temperature differences that must be satisfied in order to maintain the relative error below ten percent. A set of relevant minimum values are listed in the following table.

V [gal/min]	ΔT [°C]
1.00	2.14
0.50	2.28
0.30	2.81
0.25	3.50

Error Analysis of Heat Flux Meter Results

The heat flux results are obtained using the following equation

$$q'' = k\frac{\Delta T}{\Delta x} \tag{4}$$

Again the interest is in the relative temperatures between thermocouple junctions in a heat flux meter rather than in the measured absolute temperatures. Therefore the accuracy of temperature measurement is assumed to be equal to the resolution of the temperature measurement (ΔT_{err} = 0.150 °C). The variance of the error then can be assumed to be roughly constant. The positions of the thermocouples in the heat flux meters were recorded with an accuracy of Δx_{err} = 0.05 mm. Now assuming that the error in the position measurement is negligible, we can use the following relationships in order to get an estimate for error in the heat flux measurement [17]:

the experimental error variance

$$s^2 = \frac{\sum (T-\hat{T})^2}{(n-1)} \tag{5}$$

the estimated standard error of the heat flux is then

$$q''_{err} = \sqrt{\sigma(q'')} = \sqrt{\frac{s^2}{\sum x^2}} \tag{6}$$

The uncertainty of the value of the thermal conductivity of the aluminum plate is k_{err} = 0.006 $Wcm^{-1}{}^{o}C^{-1}$ [15]. The relative magnitude of the uncertainty of thermal conductivity of aluminum is negligible. The estimates for the variance is dependent on the test run and the heat flux meter in question. The estimates are computed with the HTF-data reduction program. Typically, the standard error of a heat flux estimate is less than 3 percent. However, the reader should note that this analysis ignores possible unknown or unexpected systematic errors caused by some technical difficulties such as an imperfect thermal contact between a thermocouple and the test plate.

Equipment Testing

Flow Field in the Test Channel

One of the design goals for the current experimental apparatus is that the flow field would reasonable well simulate a flow over a flat plate. The height and width of the test channel were chosen so that the developing boundary layers in the test channel would not interfere. The estimate was based on the calculation of a turbulent boundary layer thickness at the exit given by

$$\delta = \frac{0.37x}{Re_x^{1/5}} \tag{7}$$

The calculated estimate was checked experimentally using a hot wire anemometer probe. The velocity traverses were made at two locations. The upstream traverse was made at HFM-1 station (three inches downstream from the leading edge of the cooled test surface.) The downstream traverse was performed at HFM-7 station (three inches upstream from the exit.) The data was acquired over 1.5 seconds time interval. The length of time interval was limited by the data storage size. The sampling rate was 10 kHz, so that the velocity fluctuations up to 5000 Hz were recorded.

The results from the velocity traverse measurements are shown in Fig. 1 and Fig. 2.

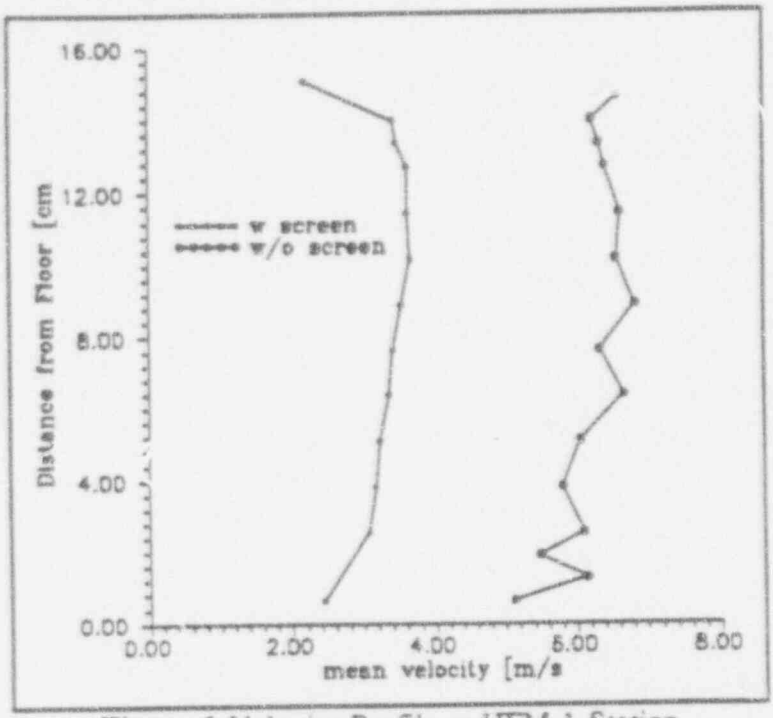

Figure 1 Velocity Profile at HFM-1 Station

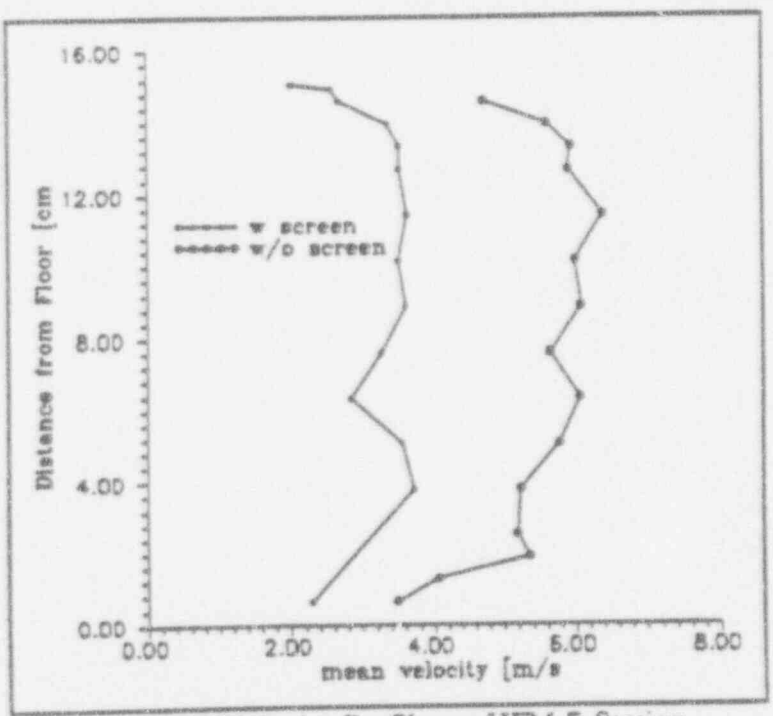

Figure 2 Velocity Profiles at HFM-7 Station

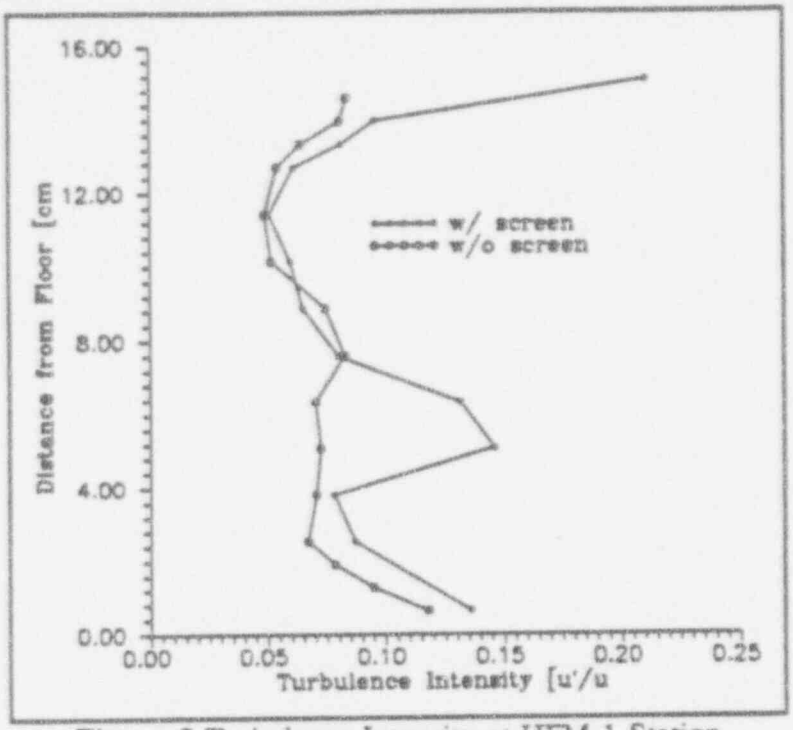

Figure 3 Turbulence Intensity at HFM-1 Station

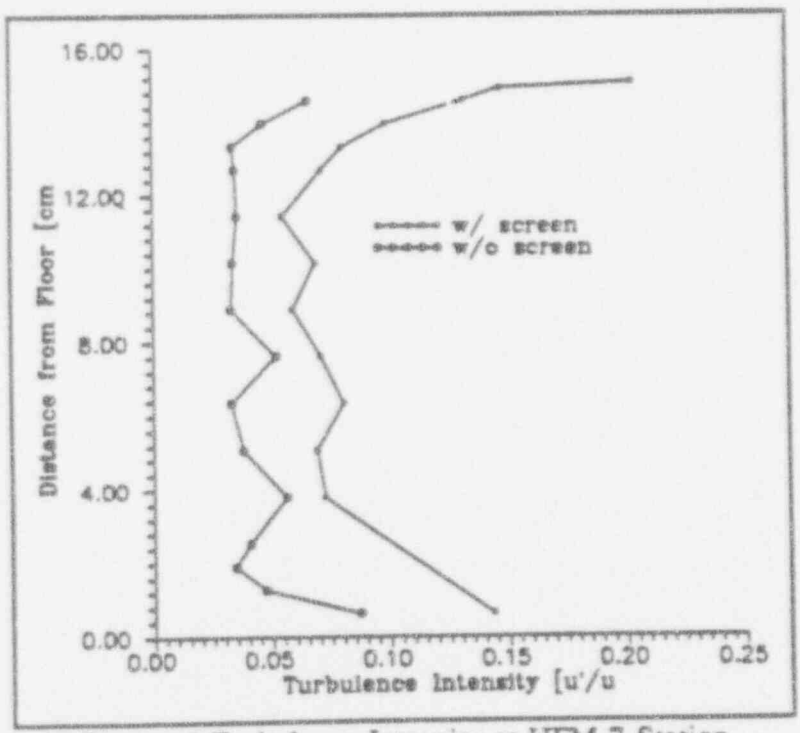

Figure 4 Turbulence Intensity at HFM-7 Station

The results confirm that the flow is still developing in the test region.

The turbulence intensity traverses were computed using the same velocity data sets as above. The turbulence intensity levels (Fig. 3 and 4) had an expected magnitude and stayed relatively constant through the test section. The fact that turbulence levels stayed under 20 percent also imply a simple hot wire probe is adequate for velocity measurements in the current research effort [18].

Sample Mass Balance and Energy Balances

A test run (70°C & 2 m/s & 0°) was made in order to check that the measured energy and mass flows were consistent. The steady state mass flow rates in and out of the mixing chamber were measured. The mixture temperature was measured 3/4" upstream from the leading edge of the test plate.

Substituting the results in the energy balance equation

$$\dot{E}_{in} = \dot{Q}_{heater} + \dot{m}_a[(T_a - T_{ref})c_{p_a} + i_g + c_{p_g}(T_{mix} - T_{ref})]_{T(y=\infty)} + \dot{m}_g[c_{p_g}(T_g - T_{ref})]$$
$$\dot{E}_{out} = \dot{m}_a[i_g + c_{p_g}(T_{mix} - T_{ref})]_{T_\infty} + \dot{m}_g[c_{p_g}(T_{mix} - T_{ref})] + \dot{m}_c[c_{p_c}(T_c - T_{ref})] \quad (8)$$